THE NASCENT PROJECT

S. Janz[1], P. Löper[1], M. Schnabel[1], M. Zacharias[2], D. Hiller[2], S. Gutsch[2], A.M. Hartel[2], C. Summonte[3], M. Canino[3], M. Allegrezza[3], S. Ossicini[4], R. Guerra[4], I. Marri[4], B. Garrido[5], S. Hernandez[5], J. López-Vidrier[5], J. Valenta[6], T. Kubera[7], M. Foti[8], C. Gerardi[8]
[1]Fraunhofer Institut für Solare Energiesysteme, [2]Universität Freiburg, [3]Consiglio Nazionale delle Ricerche – Istituto per la Microelettronica e i Microsistemi Bologna, [4]Università di Modena e Reggio Emilia, [5]Universitat de Barcelona, [6]Charles University Prague, [7]AZUR Space, [8]STMicroelectronics Catania
Corresponding author: Stefan Janz, Fraunhofer Institut für Solare Energiesysteme, Heidenhofstrasse 2, D-79110 Freiburg, Germany, Ph +49 761 4588 5261, Fax +49 761 4588 9250.

ABSTRACT: We present an overview of the project NASCEnT and the first results we were able to achieve after one year of project duration. The overall objective of the project is to develop new nano-materials with new production technologies and to fabricate silicon quantum dot (Si QD) materials for all-silicon tandem solar cells to achieve increased efficiencies. The understanding of electrical transport and recombination mechanisms in these newly developed nano-materials will enable us to design novel solar cell structures that help to overcome the efficiency limits of conventional solar cell concepts. So far we developed simple device structures and process sequences for both material systems (Si QDs in silicon oxide and silicon carbide) and tested a pin solar cell structure. Another objective of the project is to ensure the compatibility of the newly developed technologies with high-throughput processing leading to further cost-reduction. Within the scope of this project the novel concept of band gap-tuneable quantum dot superlattices is to be exploited in combination with a wafer-based high efficiency silicon solar cell as well as with a thin-film solar cell structure. The outcome of the project will be significant progress in solar cell evolution and will lead to higher efficiencies for solar cells and to ongoing cost-reductions from both a short-term and a long-term perspective.
Keywords: Quantum Dots, Nanoparticles, Devices, Tandem

1 INTRODUCTION

Crystalline silicon wafer solar cells have been dominating the photovoltaic (PV) market so far. Availability and stability of crystalline silicon and the decades of Si technology development together with the non-toxicity of the material are the main reasons for that success. Record efficiencies with up to 25 % could be shown but their maximum efficiency is limited to 29.4 % [1] due to different loss mechanisms. Without strategies to circumvent this limitation the c-Si technology will not be able to maintain its dominant role in the PV market. However, thermalisation losses e.g. can be reduced by adding a top cell with a higher band gap above a conventional silicon cell to create a tandem cell with potentially more than 40 % of efficiency. Silicon quantum dots (Si QDs) are a promising candidate for the top cell of an all-Si tandem solar cell, with a band gap that is tuneable from 1.3-1.7 eV [2, 3] by adjusting QD size. They are readily produced within a Si-based dielectric matrix by precipitation from a stack of alternating Si-rich and stoichiometric dielectric layers [4].

In order to exploit the potential of band gap engineered silicon nano-crystals for photovoltaics we formed a European consortium with 6 research institutions from Italy, Spain, Czechia and Germany together with two companies working in the solar cell and the microelectronic industry. Within the NASCEnT project we work on the following key issues that are relevant for a silicon NC solar cell. *Doping and enhanced material quality of silicon superlattices*: The combination of experiments (material fabrication and characterisation) with theoretical simulation, and comparing Si QDs superlattices in SiC, SiN_x and SiN_xO_y matrices (Si/SiC, Si/SiN_x and Si/SiN_xO_y) provide a deeper understanding of segregation, crystallisation and defect engineering. *Novel and high-throughput feasible technologies:* The technologies used to realise Si QDs in dielectric matrices are adapted to enable enhanced process throughput. Furthermore, processing is advanced in order to enable solid phase crystallisation on mid-temperature substrates (for c-Si thin-film applications). *Recombination in and charge carrier transport through doped and undoped superlattices:* Charge carrier lifetimes and mobility are key parameters for efficient carrier extraction from solar cells. Based on detailed investigations of recombination and transport processes material and device optimisation can be carried out. *Realisation of novel all-Si wafer-based and c-Si thin-film-based tandem solar cells and cost calculation:* The monolithically integrated connection of the single cells, tandem solar cell modelling and novel solar cell process sequences for all-Si tandem cells (see Figure 1) which have not yet or only in parts been investigated so far are the main focus of this work package.

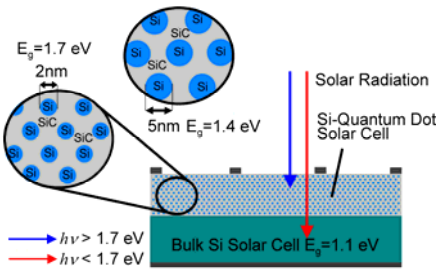

Figure 1: Schematic concept of an all-Si tandem solar cell. The bottom cell is made of bulk crystalline Si while the top cell is realised with Si quantum dots in a SiO_2 or a SiC matrix.

Device parts such as emitters, passivation layers, insulating layers and tunnel diodes for tandem cell integration are developed within this project. In this publication we show some highlights of the promising results we have achieved after just one year of project

duration.

2 METHODS

2.1 Theoretical Studies and Modeling

Working within the DFT (Density Function Theory) – LDA (Local Density Approximation) framework, we have recently investigated structural and opto-electronic properties of bare Si-NCs (with a diameter ranging from 0.2 to 1.5 nm), of H- and OH-terminated Si-NCs, and of Si-NCs embedded in a SiO_2 matrix. Different conditions of size, passivation, strain, and symmetry have been considered in order to investigate optical absorption and emission response.

Previous many-body calculations on Si-NCs reported fundamental gaps and absorption spectra very close to the DFT-RPA (Random Phase Approximation) calculated ones. We have verified this statement for the Si_{10} and amorphous-Si_{10} embedded NCs, showing that self-energy (calculated by including quasi-particle effects in the energy spectrum working within the G0W0 approximation) and electron-hole Coulomb corrections (calculated within the many body perturbation theory MBPT by solving the Bethe-Salpeter equation) nicely cancel each other out (the total correction to the gap in that case was smaller than 0.1 eV) when the local-field effects (LFE) are neglected. These considerations justify the choice of DFT-LDA for our calculations, allowing a good compromise between accuracy and computational effort.

2.2 Material Development and Characterisation

Superlattices consisting of silicon rich silicon oxynitride (SRON) and stoichiometric silicon dioxide (SiO_2) [4] were deposited on n-type (100)-Si substrates using an Oxford Instruments "Plasmalab 100" Plasma Enhanced Chemical Vapour Deposition (PECVD) system with a 13.56 MHz driven parallel plate reactor. Argon diluted SiH_4 and N_2O were used as precursor gases for both types of layers. By increasing the flow ratio $\Gamma = [N_2O]/[SiH_4]$ from 5 to 660, the film growth can be changed from SRON to stoichiometric SiO_2. Further experimental details can be found in Ref. [5]. Ex-situ spectroscopic ellipsometry confirmed a low deposition rate in the range of only 1.5 to 2.5 Å/s and an excellent homogeneity in the sub-percent range across a 4" wafer. The stochiometry was determined by XPS on thick layers of the respective films. Multilayers consisting of 20 bilayers were sandwiched between 10 nm SiO_2 buffer and capping layers. The thickness of the SRON was changed from 2.5 nm to 7 nm in steps of 1.5 nm whereas the SiO_2 barrier layer thickness was fixed at 4 nm. Hereafter, the samples were annealed at 1100 °C for 1 h in N_2 ambient using a quartz tube furnace. Then, the samples were passivated by forming gas annealing at 450 °C for 1 h. PL was measured at room temperature with a LN2-cooled CCD camera attached to a single grating monochromator using a HeCd laser (325 nm) as excitation source. Transmission electron microscopy (TEM) was performed with a JEOL J2010F (S)TEM operating at 200 kV. The energy filtered images (EFTEM) were used to estimate the Si QD size. Cross section sample preparation was done by conventional mechanical polishing and final Ar beam thinning.

For the development of SiC based quantum dot absorbers we focused on the determination of optical properties and in particular the absorption coefficient. We used a multichamber PECVD system by MVSystem-Elettrorava with parallel plate configuration, driven at 13.56 MHz. The gas mixture used was a H_2 diluted silane – methane gas mixtures with $\Gamma = [SiH4]/[CH4]$ from 44 to 0, that allows a variation of the composition layer from pure silicon to stoichiometric SiC. Gas pressure and substrate temperature were 0.95 hPa and 350 °C respectively. Further details are reported in Ref. [6]. The SiC/SRC superlattices (SL) consisted of stoichiometric SiC (3 nm) and Silicon Rich Carbide ($Si_{0.95}C_{0.05}$) layers with thicknesses of 1 to 4 nm. The SLs were deposited on quartz substrates. The thermal treatment of the samples was done at 1100 °C. To determine layer thickness and composition we use UV-Vis Reflectance and Transmittance (R&T) spectra. The spectra are simulated using an Effective Medium Approximation (EMA) mixture of SiC, µc-Si and a-Si optical functions, and fitted to the R&T data to obtain layer thicknesses and compositions.

2.3 Device Processing

For the electrical characterisation of our continuously improved absorber materials, special devices are being prepared for determining the basic electrical properties in the dark and under illumination. Especially for silicon carbide matrix systems we had to, in a first step, understand the electrical properties of intrinsic and doped partially recrystallised films in comparison to their structure. Furthermore contacts to different metals are also investigated to determine which are suitable for the production of Ohmic and Schottky contacts (Figure 2). Intrinsic, n- and p-type a-SiC:H films were deposited using a Roth&Rau AK400 PECVD reactor. The process parameters were 65 W HF (13.56 MHz) with a plasma power density of 100 W/cm, 0.3 mbar pressure and a substrate temperature of 270 °C. Films nominally 260 nm thick were deposited for structural and optical characterisation, and transmission line model (TLM) structures, and films nominally 130 nm thick were deposited for Meier-Schroder (M-S) structures. Deposition times were kept the same for undoped and doped films. The as-deposited films were then annealed at 1000 °C for 60 mins under N_2. Afterwards the samples were metallised with M-S [7] structures to examine sheet and contact resistance respectively.

Figure 2: Sketch of a Meier-Schroder structure (yellow = film, black = metal).

As the carrier transport is expected to be strongly anisotropic due to the barrier layer concept special devices had to be designed to measure directly the horizontal [see Figure 3 (left)] and vertical [see Figure 3 (right)] electrical conductivities of the optimised multilayered systems. For each absorber material the processing chain was found to be significantly different. The wet etch resistance of SiC for example led to the introduction of a plasma etching which demands a different photoresist.

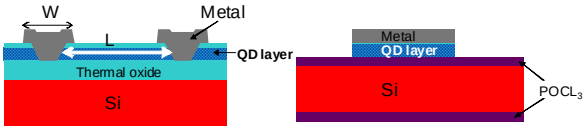

Figure 3: Test devices for determining (left) lateral and (right) vertical conductivity in quantum dot layer systems.

A first device structure to determine absorption and charge separation is shown in Figure 4. By applying a hetero structure we can investigate intrinsic absorber layers and do not have the need for diffused emitters which are an additional challenge. It enables us to realise first solar cells on both SiO_2 and SiC matrix materials even though the effect of dopants in the absorber materials is not yet well understood.

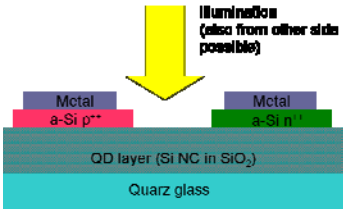

Figure 4: Sketch of a pin device with an a-Si (p++) / SiO_2: Si-QD / a-Si (n++) structure.

3 RESULTS

3.1 Modelling of Si QDs in a SiO_2 Matrix

In Figure 5 DFT calculations for Si-NCs of different size and shape, passivated with H, OH groups and embedded in a SiO_2 matrix are shown. The HOMO-LUMO gap of freestanding nano-crystals, hydrogenated (green) or hydroxidised (red) as a function of the size is plotted. The pink curve reports the average number of passivants per surface silicon.

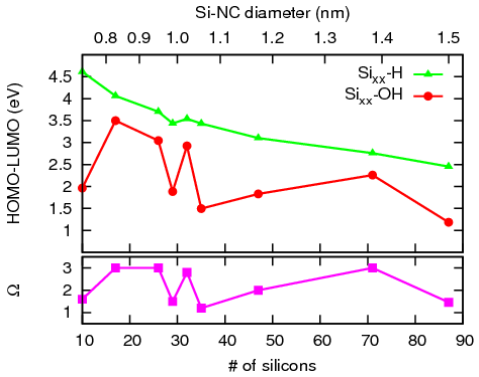

Figure 5: DFT calculations of Si-NCs of different size and shape, passivated with H and OH groups. Pink line shows number of passivants per surface Si atom *Ω*.

In Figure 6 HOMO (pink) and LUMO (blue) states are plotted at 10 % of the maximum amplitude for two nano-crystals, Si_{17} and Si_{32}, embedded in a SiO_2 matrix. The comparison between the embedded and suspended NCs shows that the matrix produces a strain on the embedded NCs. We found evidence that the amount of strain exerted on the NCs is connected to the interface configuration, in particular to the number of O atoms per interface Si. Moreover, we revealed that, while the quantum confinement (QC) dominates in H passivated NCs of all sizes, the behaviour of OH terminated and embedded NCs show a strong correlation of gap with the oxidation degree, for NCs of diameter below 2 nm (Figure 5).

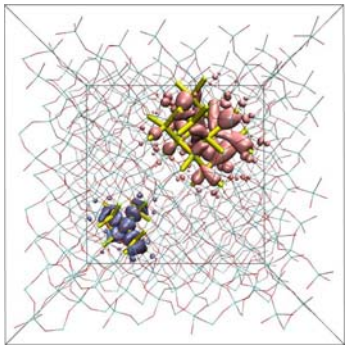

Figure 6: HOMO (pink) and LUMO (blue) plotted at 10 % of the max. amplitude for two nano-crystals, Si_{17} and Si_{32}, embedded in a SiO_2 matrix.

Concerning the applications we demonstrated that for the recombination rates the analysis of the results for the embedded NCs reveals a clear picture in which the smallest, highly oxidised, crystalline NCs, belong to the class of the most optically-active Si/SiO_2 structures, attaining impressive lifetimes of less than 1 ns, in nice agreement with experimental observations. In the case of strongly-interacting systems (i.e. when the separation between the NCs decreases below a certain limit), the overlap of the NC wavefunctions becomes relevant, promoting the tunnelling process and an indirect band gap. For more details see Ref. [8, 9]. This picture opens to the possibility of creating from one side (high rates) extremely efficient Si-based emitters, and from the other side (low rates) PV devices capable of harvesting the full solar spectrum with high yields.

3.2 Material Development and Characterisation

XPS investigations of the SRON layer (Γ = 5) resulted in 42.8 at% (Si), 46.5 at% (O) and 10.7 at% (N), corresponding to a stoichiometry of $SiO_{1.1}N_{0.25}$. For the SiO_2 film (Γ = 660) a composition of 33.3 at% (Si), 66.7 at% (O) was detected yielding a stoichiometric SiO_2 with a nitrogen content below the XPS detection limit.

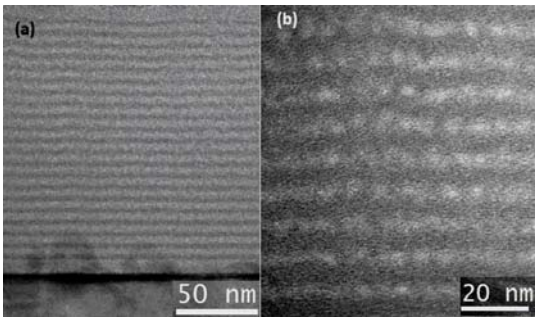

Figure 7: (a) Bright field TEM image of a superlattice sample with 4 nm of SRON annealed at 1100 °C. (b) EFTEM image at higher magnification in a thinner region of the same sample. The Si QDs are confined to 4 nm wide bands.

Figure 7 (a) shows the TEM image of a selected

superlattice with 4 nm thick layers of SRON after crystallisation at 1100 °C. The Si QDs are found within the ~4 nm thick layers of the former SiO_xN_y sublayers. The dark regions correspond to the crystallised layers and have an average thickness of 3.9 – 4.1 nm which is close to the nominal deposited values of the SiO_xN_y measured by ellipsometry. Using higher magnification EFTEM images the mean NC size was found to be 3.9 ± 0.7 nm as shown in Figure 7 (b). The size estimation of the whole sample set investigated in this study shows that the control of the Si-NC size with the former SiO_xN_y layer thickness works well for nominal layer thicknesses of up to 5.5 nm. A strong deviation from the prepared sublayer thicknesses was observed for thicknesses larger than 5.5 nm [10].

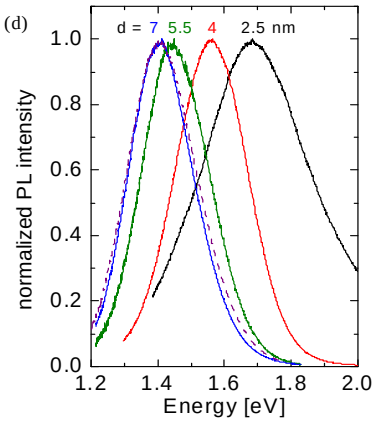

Figure 8: Normalized PL spectra of the $SiO_{1.1}N_{0.25}/SiO_2$ superlattices with different Si nano-crystal sizes after crystallisation at 1100 °C. The dotted line represents the PL spectrum of the corresponding $SiO_{1.1}N_{0.25}$ bulk film.

Figure 8 shows the normalized PL spectra for the whole set of SiO_xN_y/SiO_2 superlattices after annealing at 1100 °C. A clear shift to higher emission energies is visible by decreasing the size of the SRON layers and can be assigned to quantum confinement effects [11]. This indicates that the mean Si-NC size is limited by the SRON layer thickness. Furthermore, the spectrum of a SRON bulk film is also shown which is similar to the 7 nm superlattice sample. Hence, we can conclude that the mean Si-nc diameter is no longer controlled by SRON layer thickness above 5.5 nm as was discussed in detail before [5]. The results agree well with the TEM observations confirming that the size control is limited to Si-NC sizes smaller than 5.5 nm.

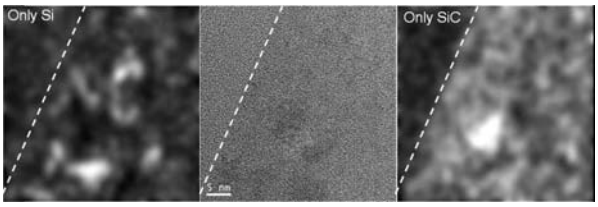

Figure 9: TEM cross section images of a 1100 °C annealed SRC $Si_{0.95}C_{0.05}$ (1 nm) / SiC (3 nm) superlattice.

In Figure 9 the TEM cross section images of a 1100 °C annealed SRC $Si_{0.95}C_{0.05}$ (1 nm) / SiC (3 nm) superlattice is shown (middle). The figures on the right and on the left were obtained by transforming the image in the middle and then anti-transforming them back after selecting the SiC and Si diffraction spots respectively, in order to separately evidence specific nano-crystals. The dashed line marks the interface with the substrate. The figure shows that in this case the initial superlattice structure is lost after annealing; however, Si nano-crystal precipitation is observed.

The EMA simulations lead to thickness values which are in excellent agreement with the measured data (with TEM). The accuracy of this method is only possible through the optical simulation of the overall composite systems, as optical effects of quantum confinement cannot be determined on extended 'bulk' materials.

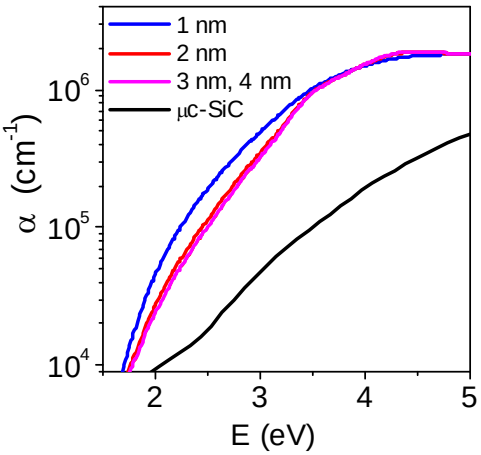

Figure 10: Absorption spectra of the Si and SiC component of several 1100°C annealed $Si_{0.95}C_{0.05}$ / SiC(3 nm) superlattices as obtained by R&T optical simulation (EMA). The curves are labelled with the SRC thickness.

Figure 10 reports the absorption of individual Si and SiC components of several annealed $Si_{0.95}C_{0.05}$/SiC(3 nm) superlattices, as obtained by R&T simulation computed using an Effective Medium Approximation (EMA) mixture of SiC, µc-Si and a-Si optical functions [12]. Although the overall absorption of the superlattices shows a blue shift with decreasing SRC thickness the absorption of the Si component itself is higher for 1 nm SRC thickness. This observation is related to the crystallised fraction in the SRC layer after annealing. Figure 10 also shows that the absorption in the material only origins from the silicon volume component and allows to exclude a contribution from the sub-band gap defect absorption in the SiC matrix component.

3.3 Contact Formation and Processing of Devices

The conductance of stoichiometric SiC films as a function of doping and contact material are summarised in Figure 11. A clear trend can be seen with doping – in all cases, p-type SiC exhibits the lowest conductance, while n-type SiC exhibits the highest conductance in all but the Al sample. The variation with contact material is not significant (as exemplified by the error bars which indicate the maximum and minimum conductance value where the bar represents the mean from two samples). The data is plotted for different contact materials simply to highlight that the trend with doping is observed on a large range of samples. It is important to mention that dopants are not only influencing the free carrier concentration in our absorber but lead also to significant changes of the solid phase crystallisation behaviour: boron doping leads to a smaller fraction of crystalline SiC

while phosphorus doping increases it. For more details see [13].

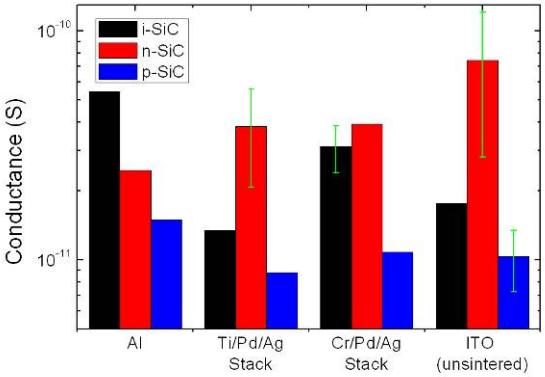

Figure 11: Conductance of SiC films measured from pad A to pad B of an M-S structure as a function of doping and contact material. Error bars indicate upper and lower value. Every bar represents an average of two samples.

The fabrication of a Si QD pin structure requires advanced structuring of the two oppositely doped a-Si layers. Two process routes have been identified: either using Si_3N_4 or using metal as an etch mask to separate the two a-Si layers without etching the QD layer itself. Several processing tests have already been successfully completed as can be seen in Figure 12. The SEM micrograph shows the still undamaged hetero emitter layer and the residuals of the masking layers with a quite accurate edge.

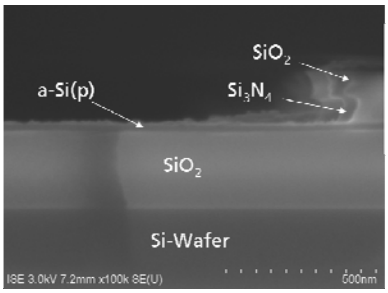

Figure 12: Scanning electron micrograph of a Si_3N_4 layer, etched by selective etching in hot H_3PO_4. This layer acts as an etch mask to separate the two oppositely doped a-Si layers.

As soon as first devices are realised we will focus on the analysis of I(V) and C(V) behaviour in dark, in order to characterise their electrical behaviour and determine the transport mechanisms involved in these systems. Furthermore, electrical characterisation under illumination (single wavelength or complete solar AM1.5 spectrum) will be performed. The photocurrent measurements will allow us to better understand the electrical and optical processes in the material and to optimise the physical parameters of the materials and the devices under study in order to improve both the absorption and charge separation in these structures.

4 CONCLUSIONS

After one year of project duration the European NASCEnT consortium has formed an excellent team which successfully combines expertise in the fields of microelectronics and photovoltaics.

First simulation results show that the computational routines developed and the obtained theoretical results can provide a genuine understanding of the dependence of the structural, opto-electronic and transport properties of semiconductor systems on their low- and nano-dimensionality.

Size controlled Si QDs in silicon oxynitride were prepared by PECVD using the superlattice approach. The size control is confirmed by TEM measurements. After annealing at temperatures of 1100 °C the samples show a very intense PL signal that blue shifts with decreasing Si QD size. This is indicative of quantum confinement effects and establishes the feasibility of size controlled Si QDs in the range between 2.5 and 5 nm using our PECVD process on a large scale. For the SiC system we developed an accurate EMA model to determine layer thicknesses out of reflection and transmission data. TEM measurements show that the initial superlattice structure is lost after annealing. However, Si NC precipitation is observed and leads to higher absorption with decreasing Si NC size.

The device processing is now at a stage where we are close to first advanced test structures for conductivity measurements in the dark and under illumination. The processing of the two different material systems led to significantly differing process chains and more additional effort than expected. We were able to develop a simple pin structure which will enable us to process intrinsic absorber materials into first solar cells.

5 ACKNOWLEDGEMENTS

The authors would like to thank their colleagues for valuable advice and discussions. We especially thank A. Leimenstoll, H.-S. Maier, S. Seitz, H. Lautenschlager, N. König and J. Löffler for processing. The research leading to these results has received funding from the European Community's Seventh Framework Programme (FP7/2007-2013) under grant agreement n°: 245977 under the project title NASCEnT. P. Löper gratefully acknowledges the scholarship support from the Reiner Lemoine Stiftung, and the ideational support from the Heinrich Böll Stiftung.

6 REFERENCES

[1] Green, M.A., Materials Science Surveys, 1987, Trans Tech Publications: Kensington, p. 99.
[2] Conibeer, G., *et al.*, Thin Solid Films, 2006, 511-2: p. 654-62.
[3] Löper, P., *et al.*, Proceedings of the 24th European Photovoltaic Solar Energy Conference, 2009, Hamburg (Germany) p. 734-738.
[4] Zacharias, M., *et al.*, Applied Physics Letters, 2002, 80(4): p. 661-3.
[5] A.M. Hartel, D. Hiller, S. Gutsch, P. Löper, S. Estradé, F. Peiró, B. Garrido, M. Zacharias, Thin Solid Films (2011), in press.
[6] C. Summonte, M. Canino, M. Allegrezza, M. Bellettato , and A. Desalvo, *"Systematic characterization of silicon nanodot absorption for third generation photovoltaics"*, this conference.
[7] Edmond, J.A., *et al.*, Journal of the Electrochemical

Society, 1988. 135(2): p. 359-62.
[8] R. Guerra, S. Ossicini, Phys. Rev. B 81, 245307(1-6) (2010).
[9] R. Guerra, M. Marsili, O. Pulci, S. Ossicini, Phys. Rev. B 84, 075342(1-7) (2011).
[10] J. López-Vidrier, S. Hernández, A. M. Hartel, D. Hiller, S. Gutsch, P. Löper, L. López-Conesa, S. Estradé, F. Peiró, M. Zacharias, B. Garrido, Energy Procedia (2011), in press.
[11] J. Heitmann, R. Scholz, M. Schmidt, M. Zacharias, J. Non-Cryst. Solids 299 (2002) p.1075.
[12] E. Centurioni, Appl. Opt. 44 (2005) 7532.
[13] M. Schnabel, A. Witzky, P. Löper, R. Gradmann, M. Künle, S. Janz, *"Electrical Properties of Recrystallised SiC Films from PECVD Precursors for Silicon Quantum Dot Solar Cell Applications"*, this conference.